Journal of Materials Chemistry B

Accepted Manuscript

ROYAL SOCIETY OF CHEMISTRY

www.rsc.org/materialsB

Graphical abstract

Preparation of magnetic metal–organic framework nanocomposites for highly specific separation of histidine-rich proteins

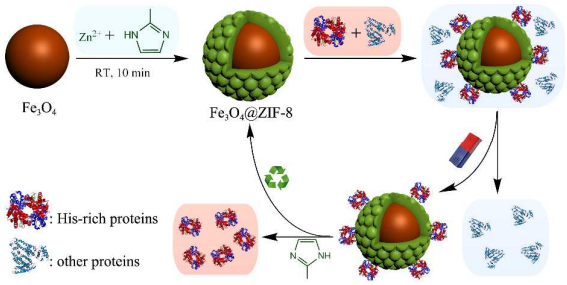

Journal Name

RSCPublishing

ARTICLE

Preparation of magnetic metal-organic framework nanocomposites for highly specific separation of histidine-rich proteins

Cite this: DOI: 10.1039/x0xx00000x

Received 00th January 2012,
Accepted 00th January 2012

DOI: 10.1039/x0xx00000x

www.rsc.org/

Jiangnan Zheng, Zian Lin,* Guo Lin, Huanghao Yang and Lan Zhang*

This work reports a novel metal–organic framework (MOF)-based metal affinity platform for the rapid and highly specific separation of histidine-rich proteins using zeolitic imidazolate framework-8 coated magnetic nanocomposites (denoted as Fe_3O_4@ZIF-8). The coating of ZIF-8 layer on Fe_3O_4 core was performed in aqueous solution at room temperature and merely took 10 minutes. The monodisperse Fe_3O_4@ZIF-8 have an average diameter of 190 nm, display superparamagnetism with a saturation magnetization value of 47.9 emu g^{-1}, and possess large external surface area of 131.0 m^2 g^{-1}. Due to the high density of low-coordinated Zn atoms on the surface of ZIF-8, Fe_3O_4@ZIF-8 exhibited large adsorption capacity for model histidine-rich protein (>6000 mg g^{-1} for bovine hemoglobin) and relatively low adsorption capacities for other proteins which containing fewer surface-exposed histidine residues. Moreover, Fe_3O_4@ZIF-8 showed excellent recyclability (more than 10 times) with high recovery (88.4 %). In addition, Fe_3O_4@ZIF-8 can be used to selectively separate hemoglobin from protein mixture and human blood samples. The good results demonstrate the potential of Fe_3O_4@ZIF-8 in the separation of histidine-rich proteins.

Introduction

Histidine (His)-rich proteins play important roles in various physiological processes, such as cellular metal homeostasis, detoxification, antimicrobial response, and intrinsic pathway of coagulation.[1] An abnormal level of His-rich proteins has been considered as an indicator for many diseases, such as malaria, chronic kidney disease, and thrombotic disorders.[2,3] However, direct analysis of these His-rich proteins in complex samples is still very challenging. Thus, the separation of His-rich proteins from biological samples is essential for ongoing proteomic and biomedical analysis. To meet this requirement, immobilized metal affinity chromatography (IMAC) and metal oxide affinity chromatography (MOAC) have been developed. However, conventional chromatography is unsuitable to directly deal with biological samples containing suspended solids and fouling components.

Magnetic nanoparticles (MNPs) have been widely applied in proteomics analysis due to their high surface to volume ratio and ease of magnetic isolation.[4] Various kinds of MNPs immobilized with metal ions have been explored to separate His-tagged proteins or natural His-rich proteins from complex samples.[5–14] For instance, Xu and co-workers developed nickel-nitrilotriacetic acid (NTA)-based MNPs for selective binding and separating of His-tagged proteins.[5,6] Chen and co-workers developed a serials of iminodiacetic acid (IDA) immobilized MNPs for depletion of His-rich bovine hemoglobin (BHb). [9–13] Yet, the synthetic routes of these IMAC–based approaches are tedious and time-consuming. As a more efficient method, several kinds of magnetic metal oxide nanocomposites have been explored to separate His-tagged proteins.[15–22] These MOAC–based MNPs, however, still suffer from drawbacks such as poor recyclability, lower saturation magnetization and severe aggregation of nanomaterials.

Metal–organic frameworks (MOFs) have attracted immense attention duo to their highly porous, excellent mechanical stability, and tunable surface properties. These unique properties make MOFs as valuable candidates in separations and purifications, which is attracting intense interest of researchers working in the fields of chemistry and materials science.[23] As a subfamily of MOFs, zeolitic imidazolate frameworks (ZIFs) have gained particular attention due to their exceptional chemical and thermal stabilities[24] and the ease of synthesis[25]. It can be expected that the external surface of ZIFs is dominated by low-coordinated Zn atoms, which can chelate with histidine resides in His-rich proteins. However, the protein-ZIFs interaction has not been investigated till now as far as we know.

In this work, a novel MOF-based metal affinity material, magnetic ZIF-8 nanocomposites (Fe_3O_4@ZIF-8) with a core–shell structure and high magnetic responsibility, was fabricated for the selective capturing of natural His-rich proteins. The nanocomposites are designed by the incorporation of rapid response toward an assistant magnetic field and high density of zinc ions on the surface, which would enable the highly efficient and facile separation of His-rich proteins. The properties of Fe_3O_4@ZIF-8 synthesized by a facile method were characterized in detail. The affinity of the nanocomposites toward several natural proteins, which contain different numbers of surface-exposed His residues, were examined. In addition, the practicability for biological applications was further assessed by isolation and depletion of hemoglobin from human whole blood.

Experimental

Materials

Ferric chloride hexahydrate ($FeCl_3 \cdot 6H_2O$), sodium acetate, sodium citrate dehydrate ($Na_3Cit \cdot 2H_2O$), ethylene glycol, and $Zn(NO_3)_2 \cdot 6H_2O$ were obtained from Sinopharm Chemical Reagent, Co., Ltd (Shanghai, China). 3-(N-morpholino)propanesulfonic acid (MOPS) and trifluoroacetic acid were obtained from Aladdin Chemistry Co., Ltd (Shanghai, China). 2-methylimidazole (HMeIM) was purchased from J&K Chemical Ltd (Shanghai, China). BHb, bovine serum albumin (BSA) and horseradish peroxidase (HRP) were purchased from Shanghai Lanji Co. Ltd. (Shanghai, China). Human serum albumin (HSA) were obtained from Wako Pure Chemical Industries Ltd. (Japan). Myoglobin from equine skeletal muscle (Mb, Sigma M1882), lysozyme from chicken egg white (Lyz, Sigma L7651) and cytochrome c from equine heart (Cyt C, Sigma C2867) were the products of Sigma-Aldrich (St. Louis, USA). Healthy human blood was kindly donated by Fujian Provincial Official Hospital (Fuzhou, China). Deionized water (18.2 MΩ cm^{-1}) was prepared with a Milli-Q water purification system (Millipore, USA). All reagents above were of analytical grade or better.

Preparation of Fe_3O_4 microspheres

$FeCl_3 \cdot 6H_2O$ (6.8 g), sodium acetate (12.0 g), $Na_3Cit \cdot 2H_2O$ (2.0 g) were dissolved in ethylene glycol (200 mL). The obtained homogeneous yellow solution was transferred to autoclave, and then heated to 200 °C for 10 h. After reaction, the product was separated with a magnet and washed with water and ethanol for several times.

Preparation of Fe_3O_4@ZIF-8

Fe_3O_4 microspheres (0.35g) were dispersed in 20 mL of 50% ethanol solution containing 2 mmol $Zn(NO_3)_2$ and 0.2 mmol HCl. Then, 40 mL of 50% ethanol solution containing 20 mmol 2-methylimidazole (HMeIM) was added to above suspension. The resulting mixture was stirred with ultrasound at room temperature for 10 min. The products were collected with a magnet and washed with ethanol and water.

Characterization

Scanning electron microscopy (SEM) images were obtained using an S-4800 TEM (Hitachi, Japan). Transmission electron microscopy (TEM) analyses were performed on a Tecnai G2 20 (FEI, USA) at 200 kV. Nitrogen adsorption and desorption isotherms were measured using an ASAP 2020 (Micromeritics, USA). The samples were degassed in a vacuum at 300 °C for 4 h prior to measurement. The surface area of the samples was estimated using the Brunauer–Emmett–Teller (BET) equation. The total pore volume, V_T, was determined using the desorption branch of the N_2 isotherm at P/P_0 = 0.991. The micropore surface area and micropore volume, S_{micro} and V_{micro}, respectively, were calculated using the t-plot method.[26] The external surface area, S_{Ext}, was calculated by subtracting S_{Micro} from S_{BET}. The pore volume and size distribution were estimated by non-local density functional theory (NLDFT) model, assuming a kernel model of N_2 at 77 K on pillared clay (cylindrical pores, NLDFT equilibrium model).[27] Fourier-transform infrared (FTIR) spectra were recorded by Nicolet 6700 spectrometer (Thermo Fisher, USA) using KBr pellets. The crystal structure of the MMN was determined by X'Pert-Pro MPD (Philips, Holland). The magnetization curves were carried out at 300 K on a superconducting quantum interference device magnetometer (SQUID) MPMS XL-7 (Quantum Design, USA).

HPLC analysis were carried out using a Shimadzu Prominence LC-20A HPLC (Kyoto, Japan) with an Agela Technologies Venusil XBP C8 (100 mm×4.6 mm, 5 μm, 300 Å) column (Tianjin, China). The proteins were analyzed under the gradient condition: gradient was carried out with buffer A (0.1% TFA aqueous solution) and buffer B (0.08% acetonitrile solution); 0-0.3 min, 30% B; 0.3-2.5 min, a linear gradient of buffer B from 30 to 40%; 2.5-6.0 min, a linear gradient of buffer B from 40 to 60% was used; the flow rate was 1.0 mL/min; column temperature was 40 °C. The injected sample volume was 20 μL, and the samples were detected using a UV detector (280 nm for BSA, HSA, and Lyz; 406 nm for BHb, Mb, Cyt C and HRP). Quantitative analysis of the protein solutions were performed from a linear calibration curve of peak area versus concentration. Electrophoresis of proteins was performed using regular sodium dodecyl sulfate polyacrylamide gel electrophoresis (SDS-PAGE) using the Mini-protean II system (Bio-Rad, USA) with 12% running and 5% stacking gels. Proteins were stained with Coomassie Brilliant Blue R-250.

In-vial adsorption and separation of proteins

The adsorption experiments were conducted in a centrifuge tube at room temperature. All sample solutions were prepared in binding buffer (30 mM MOPS containing 0.45 M NaCl, pH 7.0).

In the isothermal adsorption experiments, 0.2 mg of Fe_3O_4@ZIF-8 was vortex-mixed with 2.0 mL of BHb solutions

at different concentrations for 10 min in the tube. The nanocomposite-proteins conjugates were magnetically isolated by magnet. Then the supernatants were collected for HPLC analysis. The equilibrium adsorption capacity (Q_e, mg g^{-1}) was calculated according to

$$Q_e = \frac{(C_0 - C_e)}{m} V \quad (1)$$

where C_0 is the initial protein concentration (μg mL^{-1}), C_e is the supernatant protein concentration (μg mL^{-1}), V is the volume of protein solution (mL) and m is the weight of the Fe_3O_4@ZIF-8 (g). The adsorption isotherms were fitted by the Langmuir model (Equation 2) and Freundlich model (Equation 3),

$$\frac{C_e}{Q_e} = \frac{1}{bQ_m} + \frac{1}{Q_m} C_e \quad (2)$$

$$\log Q_e = \log K_f + \frac{1}{n} \log C_e \quad (3)$$

where b is the Langmuir constant that directly relates to the adsorption affinity (L mg^{-1}), Q_m is the saturated capacity (mg g^{-1}), respectively. Q_m and b can be calculated by plotting C_e/Q_e as a function of C_e. K_f is Freundlich isotherm constant (mg g^{-1}), n is a heterogeneity parameter.

In the kinetic adsorption experiment, 0.20 mg of Fe_3O_4@ZIF-8 was incubated with 2 mL of BHb solution for different incubation times. The adsorption kinetics was fitted by the pseudo-second-order kinetic model (Equation 4)

$$\frac{t}{Q_t} = \frac{1}{k_2 Q_e^2} + \frac{t}{Q_e} = \frac{1}{V_0} + \frac{t}{Q_e} \quad (4)$$

where Q_t is the adsorption capacity (mg g^{-1}) after shaking a time of t (min), k_2 is the rate constant (g mg^{-1} min^{-1}), and V_0 is the initial adsorption rate (mg g^{-1} min^{-1}), respectively.

In the specific adsorption experiments, 0.20 mg of Fe_3O_4@ZIF-8 was incubated with 0.4 mL of protein mixture containing CytC (250 μg mL^{-1}), Lyz (250 μg mL^{-1}), BSA (2000 μg mL^{-1}) and BHb (2000 μg mL^{-1}) for 10 min. After magnetic separation, the supernatants were collected. The captured proteins were eluted with 0.2 M HMeIM solution containing 0.45 M NaCl. The supernatants and the eluates were analyzed by HPLC.

Reusability of Fe_3O_4@ZIF-8

0.3 mg of Fe_3O_4@ZIF-8 was incubated with 0.3 mL of BHb solution (1000 μg mL^{-1}) for 10 min. After magnetic separation, the supernatants were collected. The captured proteins were eluted with 0.2 M HMeIM solution containing 0.45 M NaCl. Then, the Fe_3O_4@ZIF-8 were vortexed with 0.1 mL of newly prepared solution containing $Zn(NO_3)_2$ (0.05 M) and HMeIM (0.1 M) for 1 min. After washed with water for several times, the recovered product was reused for protein adsorption.

Real sample analysis

1.0 mL of 100-fold human whole blood sample diluted with binding buffer was incubated with 0.4 mg of Fe_3O_4@ZIF-8 for 10 min, then the captured species were eluted as mentioned above. Finally, the diluted blood sample, supernatant, and eluent were collected and analyzed by SDS-PAGE.

Results and discussion

Preparation and characterization of the Fe_3O_4@ZIF-8

The preparation of Fe_3O_4@ZIF-8 with a core–shell structure is illustrated in Fig. 1. Firstly, the citrate-stabilized Fe_3O_4 cores were synthesized via a reported solvothermal method with some modifications.[28] Then, Fe_3O_4@ZIF-8 were prepared by mixing with $Zn(NO_3)_2$ and HMeIM solution in ethanol–water system at room temperature (RT) for 10 minutes.

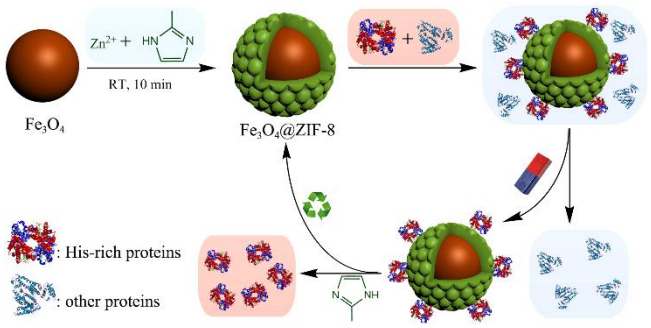

Fig. 1 Preparation of Fe_3O_4@ZIF-8 and the magnetically recyclable His-rich protein separation process.

The monodisperse core–shell structure of Fe_3O_4@ZIF-8 was verified by SEM and TEM. SEM image (Fig. 1A) showed that Fe_3O_4@ZIF-8 were nearly spherical in shape with an average diameter of 190 nm. Meanwhile, TEM image (Fig. 1B) clearly indicated the formation of ZIF-8 shell with thicknesses of *ca.*25 nm surrounding the Fe_3O_4 core. SEM and TEM images revealed the ZIF-8 shells with rough surface are composed of numerous ZIF-8 nanocrystals.

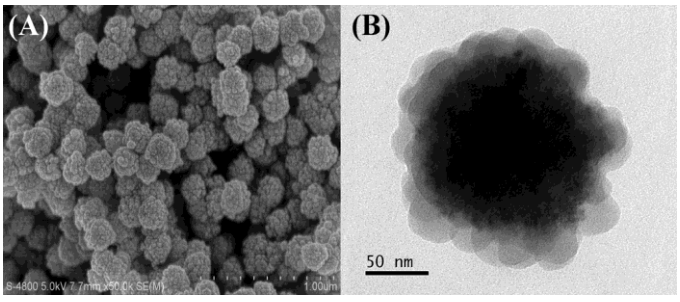

Fig. 2 SEM (A) and TEM (B) images of Fe_3O_4@ZIF-8.

The crystalline structure of Fe_3O_4@ZIF-8 is confirmed by XRD measurement (Fig. 3A). The XRD pattern of Fe_3O_4@ZIF-8 can be assigned to a superposition of characteristic peaks of face-centered cubic Fe_3O_4 (JCPDS card 19-629) and simulated pattern of the published ZIF-8 structure data.[24] Furthermore, the

mean crystallite size in the ZIF-8 shells were estimated from Debye–Scherrer's equation, and calculation for the strongest peak at 7.3° gave size of 24 nm for ZIF-8 nanocrystals, which consisted with the TEM result.

FT-IR spectrum of Fe_3O_4@ZIF-8 is presented in Fig. 3B, where Fe_3O_4 microspheres were also used as reference material. Compared to the spectrum of Fe_3O_4 microspheres, the spectrum of Fe_3O_4@ZIF-8 displays additional absorption adsorption bands which are associated with the ZIF-8 structure.[29] The bands at 3136 and 2930 cm^{-1} are attributed to the aromatic and the aliphatic C–H stretch mode, respectively. The board band centered at 1420 cm^{-1} and bands in the spectral region of 900–1330 cm^{-1} could be assigned to the stretching and plane bending of imidazole ring, respectively. The band at 422 cm^{-1} is attributed to the characteristic Zn–N stretch mode. Overall, the FT-IR spectra also confirmed the formation of ZIF-8 shells.

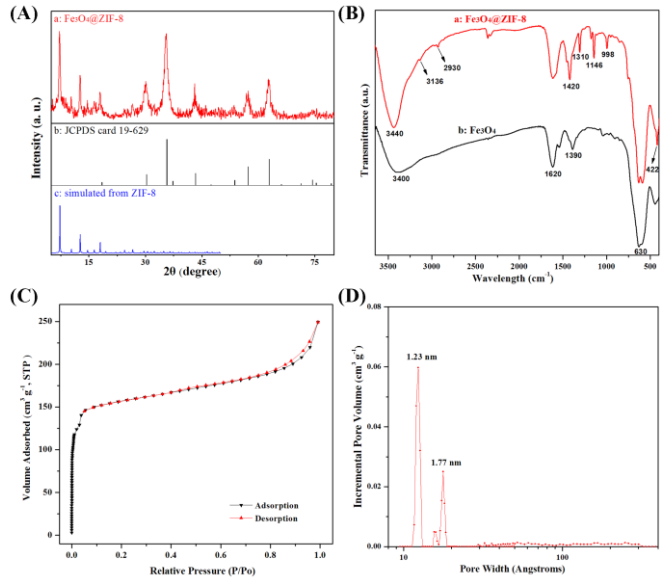

Fig. 3 (A) XRD pattern of Fe_3O_4@ZIF-8 (a), the standard diffraction lines of Fe_3O_4 (JCPDS card 19-629) (b) and simulated pattern of the published ZIF-8 structure data[24] (c); (B) FTIR spectra of Fe_3O_4@ZIF-8 and Fe_3O_4 microspheres; (C) N_2 sorption–desorption isotherms of Fe_3O_4@ZIF-8 at 77 K; (D) pore size distribution calculated by NLDFT model.

The textural properties of the Fe_3O_4@ZIF-8 were studied by the N_2 adsorption-desorption at 77 K, as shown in Fig. 3C. The isotherms of Fe_3O_4@ZIF-8 displayed a steep increase at low relative pressures (P/P_0<0.1), indicating their high microporous surface area. The isotherms also exhibit some nitrogen uptake as a kind of hysteresis at 0.4<P/P_0<1.0, which could be due to the presence of mesopores/macropores formed by the stacking of microspheres. The pore-diameter distribution of Fe_3O_4@ZIF-8 as estimated from a NLDFT model gave a pore diameter of 12.3 Å (Fig. 3D), which is close to the pore diameter (11.6 Å) of the sodalite cage in pristine ZIF-8.[24] The BET surface area of Fe_3O_4@ZIF-8 was determined to be 528.1 $m^2\ g^{-1}$ which is lower than pure ZIF-8 (1630 $m^2\ g^{-1}$) because of the contributions of non-porous Fe_3O_4 cores. A total pore volume of 0.386 $cm^3\ g^{-1}$ containing 47.9% micropore was also obtained. On account of micropores are not accessible for proteins, the external surface area is a more important parameter. The external surface area of Fe_3O_4@ZIF-8 calculated from the t-plot is 131.0 $m^2\ g^{-1}$, which is larger than MOAC–based MNPs[22] and would be beneficial to achieve high protein adsorption.

The magnetic properties of Fe_3O_4@ZIF-8 were studied using a SQUID at 300 K (Fig. 4). The magnetic hysteresis curves of Fe_3O_4 and Fe_3O_4@ZIF-8 possess a typical superparamagnetic feature (nearly zero coercivity and nearly no remanence effect) when the applied magnetic field is removed. The saturation magnetization (Ms) of Fe_3O_4@ZIF-8 is 47.9 emu g^{-1} at 300 K, which endued Fe_3O_4@ZIF-8 with a fast response to an external magnetic field. As the inset in Fig. 4 shows, the well dispersed Fe_3O_4@ZIF-8 in aqueous solution can be quickly attracted to the wall of the vial by an applied magnetic field and can be redispersed by shaking.

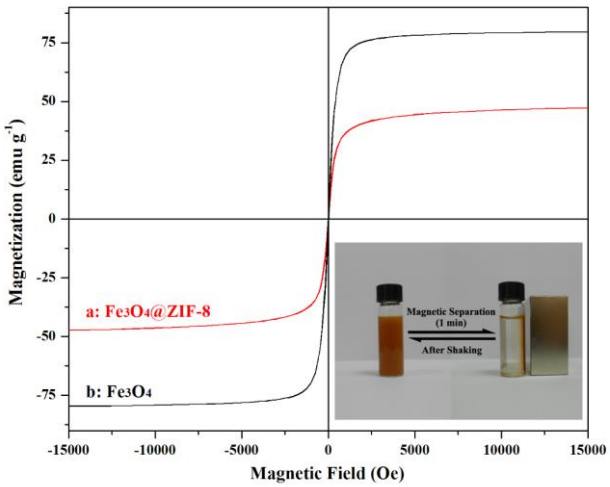

Fig. 4 Hysteresis loops of Fe_3O_4@ZIF-8 and Fe_3O_4 microspheres at 300K. The inset shows the magnetic separation behavior of Fe_3O_4@ZIF-8.

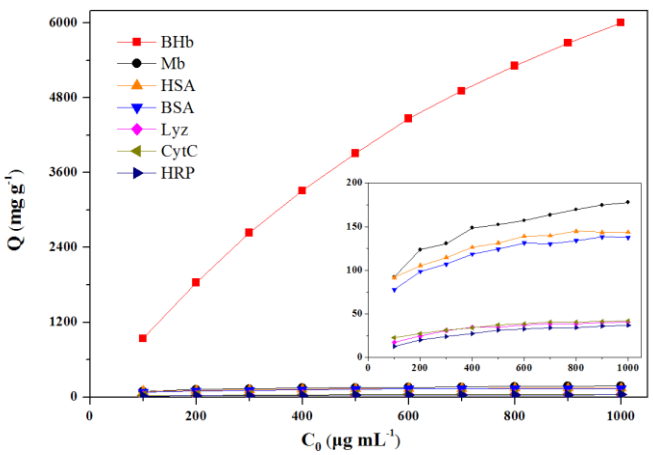

Fig. 5 Adsorption isotherms of proteins (BHb, BSA, HSA, Mb, Cyt C, Lyz and HRP) onto Fe_3O_4@ZIF-8.

Binding properties of Fe_3O_4@ZIF-8

To evaluate the selectivity of Fe_3O_4@ZIF-8 for His-rich proteins, BHb, Mb, BSA, HSA, Lyz, Cyt C and HRP were chosen as model proteins. BHb is a well-known His-rich protein containing 15 surface-exposed His residues, while other proteins possess less or none surface-exposed His residues (Table 1). To make the metal ion-histidine interaction play a dominant role in protein adsorption, a neutral buffer (30 mM MOPS containing 450 mM NaCl, pH 7) was employed. As expected, the adsorption capacities have the following order: BHb >> Mb ≈ BSA ≈ HSA > Cyt C ≈ Lyz ≈ HRP, respectively (Fig. 5), in accordance with the number of surface-exposed His residues. The Langmuir and Freundlich adsorption models were applied to describe the equilibrium isotherms. All adsorption isotherms of Mb, BSA, HSA, Cyt C, Lyz and HRP are consistent with Langmuir model. Langmuir model for these proteins appears to be more suitable than Freundlich model. The adsorption isotherm behavior of BHb is apparently different from other proteins. Instead of with the Langmuir model, the adsorption isotherm of BHb fit perfectly with the Freundlich model. 1/n is a measure of the surface heterogeneity ranging between 0 and 1. The smaller 1/n, the greater the expected heterogeneity. Thus the calculated value of 0.300 in the case of BHb indicative of an energetically heterogeneous surface.[30] The different adsorption behavior for BHb might be due to the extremely rough surface of Fe_3O_4@ZIF-8 and the multisite interaction between BHb molecule and Fe_3O_4@ZIF-8. It is worthy of note that the binding capacity for BHb reached >6000 mg g^{-1}, which is greater than any other previously reported (Table 2).

Table 1. A summary of the fitted parameters of the protein adsorption equilibrium on the Fe_3O_4@ZIF-8.

Name	Mw (kDa)	pI	PDB code	Surface-exposed His residues[a]	Langmuir model			Freundlich model		
					Q_m (μg g^{-1})	B (L g^{-1})	R^2	Log K_f (μg g^{-1})$^{(1-1/n)}$	1/n	R^2
BHb	64.5	6.8	2QSS	15	6198	190.5	0.9807	3.011	0.300	0.9998
Mb	17.7	7.3	1YMB	4	190.8	88.1	0.9951	1.594	0.223	0.9834
HSA	66.6	4.7	1AO6	3	154.3	63.9	0.9976	1.658	0.173	0.9789
BSA	66.7	4.7	3V03	4	149.0	78.8	0.9979	1.522	0.213	0.9802
Cyt C	12.4	10.6	1HRC	0	47.5	128.0	0.9972	0.847	0.265	0.9896
Lyz	14.3	11.4	1LYZ	0	47.1	156.3	0.9981	0.605	0.346	0.9385
HRP	44	5.7	1HCH	0	46.4	249.2	0.9980	0.282	0.440	0.9630

a: The surface-exposed His residues were calculated by GETAREA 1.1 software[31] based on the protein crystal structure data from Protein Data Bank (PDB).[32] See the supporting information for the detailed analysis of surface-exposed His residues of proteins.

Table 2. Properties of different adsorbents for BHb capture

adsorbent	Size	Functionalization time	Capacity (mg g^{-1})	Capture time	Recyclability
Cu-IDA-silica-coated Fe_3O_4[9]	350 nm	>3 days	419	5 h	5 cycles (15 % Loss)
Fe_3O_4@PVBC@IDA-Ni [13]	300 nm	>1 day	1988	1 h	4 cycles (30 % Loss)
Fe_3O_4@SiO_2@IL[33]	270 nm	>4 days	2150	15 min	8 cycles (20 % Loss)
$CuFe_2O_4$ MNCs[22]	170 nm	needless	4175	10 min	5 cycles (25 % Loss)
Fe_3O_4@ZIF-8 (this work)	190 nm	10 min	>6000	10 min	10 cycles (4 % Loss)

The adsorption kinetics of BHb onto Fe_3O_4@ZIF-8 at pH 7 is presented in Fig. 6A. Fe_3O_4@ZIF-8 displayed a fast adsorption rate in the first 7 min, and the equilibrium was almost achieved within 10 min, which is very favorable for the protein separation. As shown in Fig. 6B, the adsorption kinetic fit well with the pseudo-second-order model (R^2=0.9990), indicating that the chemical interactions were possibly involved in the adsorption processes.[34] Moreover, the fast initial adsorption rate (>5440 mg g^{-1} min^{-1}) and high adsorption capacity (6222 mg g^{-1}) could be ascribed to a large external surface area of Fe_3O_4@ZIF-8 and high density of zinc (II) ions on the surface.

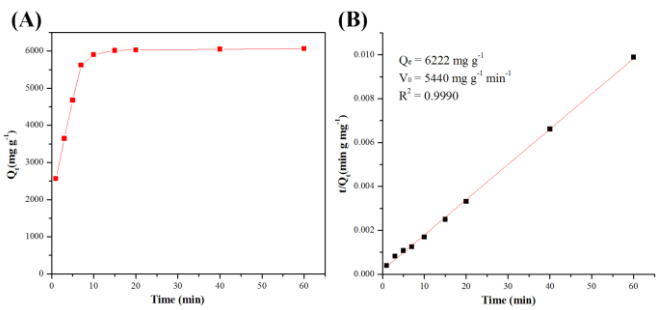

Fig. 6 (A) Adsorption kinetics of BHb (1000 μg mL^{-1}) onto Fe_3O_4@ZIF-8; (B) Fitting of the adsorption kinetics by using the pseudo-second-order kinetics model.

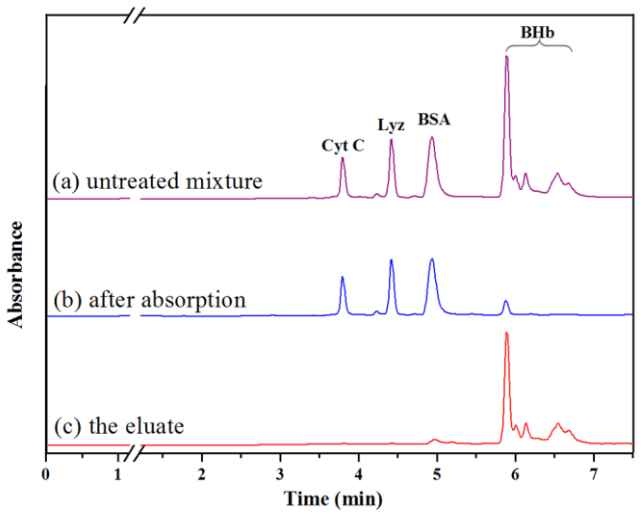

Fig. 7 HPLC chromatograms of unreacted protein mixture of BHb, BSA, CytC and Lyz with a mass ratio of 8:8:1:1 (a), the supernatant treated with Fe_3O_4@ZIF-8 (b), and the eluate from Fe_3O_4@ZIF-8–proteins conjugates (c).

Quantitative assay of mixed adsorption using HPLC

To further inspect the specificity of the Fe_3O_4@ZIF-8 for the separation of His-rich protein, a protein mixture of BHb, BSA, CytC and Lyz with a mass ratio of 8:8:1:1 was adopted. Fig. 7a shows the HPLC chromatogram of the initial protein mixture. After treating with Fe_3O_4@ZIF-8, 89.7% BHb was removed from the mixture with minor loss of CytC, Lyz, and BSA (94.8%, 95.1%, and 92.7% remained, respectively) (Fig. 7b). The captured BHb on Fe_3O_4@ZIF-8 can be eluted by 0.2 M HMeIM solution, and 78.5% BHb was recovered in the eluent (Fig. 7c).

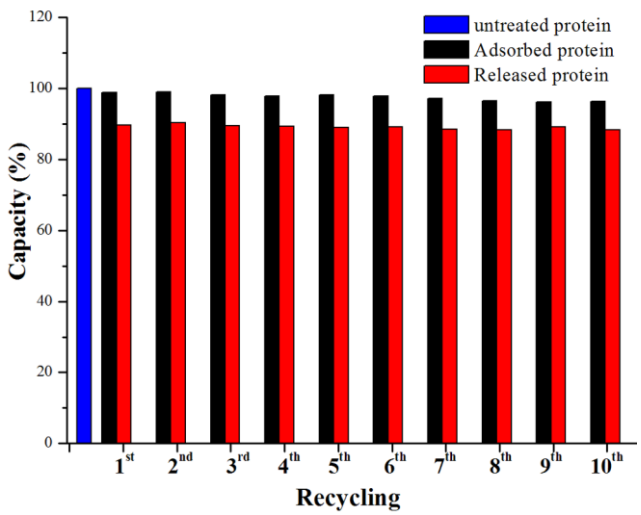

Fig. 8 The relative BHb adsorption capacity and eluted amount of the Fe_3O_4@ZIF-8 reused up to 10 times.

The recyclability of Fe_3O_4@ZIF-8 was also tested. As shown in the Fig. 8, the relative adsorption capacity and release percentage for the reused Fe_3O_4@ZIF-8 (96.3% and 88.4%, respectively) were almost unchanged after ten cycles of reuse, indicating the excellent recyclability. The result is also better than that of the literatures (Table 2). In addition, the Fe_3O_4@ZIF-8 showed acceptable preparation reproducibility with a batch-to-batch relative standard deviation of 6.3% (n=5) for the binding of BHb.

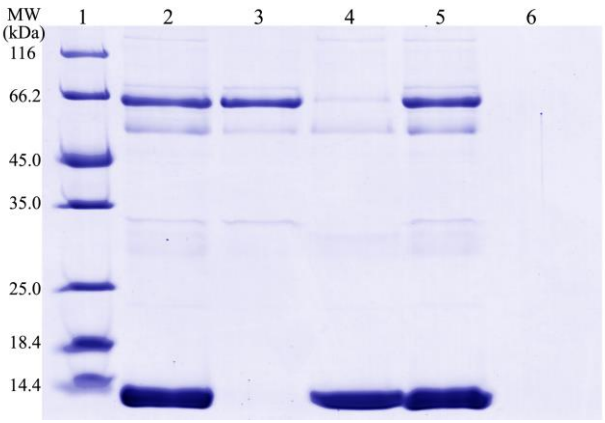

Fig. 9 SDS-PAGE analysis of human whole blood. Lane 1, marker; lane 2, 100-fold human whole blood; lane 3, the supernatant after treatment with Fe_3O_4@ZIF-8; lane 4, the eluate from lane 3; lane 5 the supernatant after treatment with Fe_3O_4 microspheres; lane 6, the eluate from lane 5.

Application

The human blood sample was used to further evaluate the practicability of Fe_3O_4@ZIF-8 in a real biological sample. As presented in Fig. 9, human whole blood (lane 2) revealed several major bands, which were mainly attributed to HSA and human hemoglobin (HHb). After treatment with Fe_3O_4@ZIF-8, all HHb was removed (lane 3) and other proteins including HSA were almost reserved. Moreover, HHb reappeared with a high content in the eluent of Fe_3O_4@ZIF-8-proteins conjugates (lane 4). More detailed information of these eluted proteins was analyzed by LC-MS/MS, and listed in Table S2†. In contrast, Fe_3O_4 microspheres didn't show any adsorption for all proteins (lane 5), and none of protein bands were found in the eluent (lane 6). Overall, the SDS-PAGE analysis indicated the practicality of Fe_3O_4@ZIF-8 for the selective depletion of high-abundance hemoglobin in blood samples.

Conclusions

In summary, we demonstrated the first example of MOF-based platform for the rapid and highly specific separation of histidine-rich proteins. Monodisperse Fe_3O_4@ZIF-8 were synthesized at room temperature and merely took 10 minutes. Due to the high density of low-coordinated Zn atoms on the surface of ZIF-8, Fe_3O_4@ZIF-8 exhibited large adsorption capacity and specificity to BHb at a physiological environment. Furthermore, the Fe_3O_4@ZIF-8 showed excellent recyclability with high recovery. In addition, Fe_3O_4@ZIF-8 can be used to selectively separate hemoglobin from human blood samples. It is expected that the Fe_3O_4@ZIF-8 could be promising affinity materials in His-rich and His-tagged protein analysis.

Acknowledgements

This study was supported by the National Natural Science Foundation of China (21375018 and 21275029), National Science Foundation for Fostering Talents in Basic Research of China (No. J1103303), the National Natural Science Funds for Distinguished Young Scholar (21125524), the Natural Science Foundation of Fujian Province (2014J01402), and the Program for Changjiang Scholars and Innovative Research Team in University (No. IRT1116).

Notes and references

Ministry of Education Key Laboratory of Analysis and Detection for Food Safety, Fujian Provincial Key Laboratory of Analysis and Detection Technology for Food Safety, College of Chemistry, Fuzhou University, Fuzhou, Fujian, 350002, China.

E-mail: zianlin@fzu.edu.cn (Z.A. Lin); zlan@fzu.edu.cn (L.Zhang); Fax: +86-591-22866135

† Electronic Supplementary Information (ESI) available. See DOI: 10.1039/b000000x/

1. M. Rowinska-Zyrek, D. Witkowska, S. Potocki, M. Remelli, and H. Kozlowski, *New J. Chem.*, 2013, **37**, 58–70.
2. D. J. Sullivan, I. Y. Gluzman, and D. E. Goldberg, *Science*, 1996, **271**, 219–222.
3. A. L. Jones, M. D. Hulett, and C. R. Parish, *Immunol. Cell Biol.*, 2005, **83**, 106–118.
4. Y. Li, X. M. Zhang, and C. H. Deng, *Chem. Soc. Rev.*, 2013, **42**, 8517–8539.
5. C. J. Xu, K. M. Xu, H. W. Gu, X. F. Zhong, Z. H. Guo, R. K. Zheng, X. X. Zhang, and B. Xu, *J. Am. Chem. Soc.*, 2004, **126**, 3392–3393.
6. C. J. Xu, K. M. Xu, H. W. Gu, R. K. Zheng, H. Liu, X. X. Zhang, Z. H. Guo, and B. Xu, *J. Am. Chem. Soc.*, 2004, **126**, 9938–9939.
7. E. J. Cho, S. Jung, K. Lee, H. J. Lee, K. C. Nam, and H.-J. Bae, *Chem. Commun.*, 2010, **46**, 6557–6559.
8. H. Y. Xie, R. Zhen, B. Wang, Y. J. Feng, P. Chen, and J. Hao, *J. Phys. Chem. C*, 2010, **114**, 4825–4830.
9. M. Zhang, D. Cheng, X. W. He, L. X. Chen, and Y. K. Zhang, *Chem. Asian J.*, 2010, **5**, 1332–1340.
10. M. Zhang, X. W. He, L. X. Chen, and Y. K. Zhang, *J. Mater. Chem.*, 2010, **20**, 10696–10704.
11. M. Zhang, X. W. He, L. X. Chen, and Y. K. Zhang, *Nanotechnology*, 2011, **22**, 065705.
12. G. Q. Jian, Y. X. Liu, X. W. He, L. X. Chen, and Y. K. Zhang, *Nanoscale*, 2012, **4**, 6336–6342.
13. J. L. Cao, X. H. Zhang, X. W. He, L. X. Chen, and Y. K. Zhang, *J. Mater. Chem. B*, 2013, **1**, 3625–3632.
14. Y. T. Zhang, D. Li, M. Yu, W. F. Ma, J. Guo, and C. C. Wang, *ACS Appl. Mater. Interfaces*, 2014, **6**, 8836–8844.
15. I. S. Lee, N. Lee, J. Park, B. H. Kim, Y.-W. Yi, T. Kim, T. K. Kim, I. H. Lee, S. R. Paik, and T. Hyeon, *J. Am. Chem. Soc.*, 2006, **128**, 10658–10659.
16. S.-Y. Huang and Y.-C. Chen, *Anal. Chem.*, 2013, **85**, 3347–3354.
17. M. F. Shao, F. Y. Ning, J. W. Zhao, M. Wei, D. G. Evans, and X. Duan, *J. Am. Chem. Soc.*, 2011, **134**, 1071–1077.
18. Z. Liu, M. Li, F. Pu, J. S. Ren, X. J. Yang, and X. G. Qu, *J. Mater. Chem.*, 2012, **22**, 2935–2942.
19. J. Chun, S. W. Seo, G. Y. Jung, and J. Lee, *J. Mater. Chem.*, 2011, **21**, 6713–6717.
20. Z. Liu, M. Li, X. J. Yang, M. L. Yin, J. S. Ren, and X. G. Qu, *Biomaterials*, 2011, **32**, 4683–4690.
21. J. Lee, S. Y. Lee, S. H. Park, H. S. Lee, J. H. Lee, B.-Y. Jeong, S.-E. Park, and J. H. Chang, *J. Mater. Chem. B*, 2013, **1**, 610–616.
22. J. N. Zheng, Z. A. Lin, W. Liu, L. Wang, S. Zhao, H. H. Yang, and L. Zhang, *J. Mater. Chem. B*, 2014, **2**, 6207–6214.
23. J.-R. Li, J. Sculley, and H.-C. Zhou, *Chem. Rev.*, 2011, **112**, 869–932.
24. K. S. Park, Z. Ni, A. P. Côté, J. Y. Choi, R. Huang, F. J. Uribe-Romo, H. K. Chae, M. O'Keeffe, and O. M. Yaghi, *Proc. Natl. Acad. Sci.*, 2006, **103**, 10186–10191.
25. Y. C. Pan, Y. Y. Liu, G. F. Zeng, L. Zhao, and Z. P. Lai, *Chem. Commun.*, 2011, **47**, 2071–2073.
26. B. C. Lippens and J. H. de Boer, *J. Catal.*, 1965, **4**, 319–323.
27. M. L. Occelli, J. P. Olivier, J. A. Perdigon-Melon, and A. Auroux, *Langmuir*, 2002, **18**, 9816–9823.
28. J. N. Zheng, Y. Xiao, L. Wang, Z. A. Lin, H. H. Yang, L. Zhang, and G. N. Chen, *J. Chromatogr. A*, 2014, **1358**, 29–38.
29. Y. Hu, H. Kazemian, S. Rohani, Y. N. Huang, and Y. Song, *Chem. Commun.*, 2011, **47**, 12694–12696.
30. A. P. Serro, K. Degiampietro, R. Colaço, and B. Saramago, *Colloids Surfaces B Biointerfaces*, 2010, **78**, 1–7.
31. R. Fraczkiewicz and W. Braun, *J. Comput. Chem.*, 1998, **19**, 319–333.
32. H. M. Berman, J. Westbrook, Z. Feng, G. Gilliland, T. N. Bhat, H. Weissig, I. N. Shindyalov, and P. E. Bourne, *Nucleic Acids Res.*, 2000, **28**, 235–242.
33. Y. Wei, Y. Li, A. Tian, Y. Fan, and X. Wang, *J. Mater. Chem. B*, 2013, **1**, 2066–2071.
34. C. M. Dai, J. Zhang, Y. L. Zhang, X. F. Zhou, Y. P. Duan, and S. G. Liu, *Chem. Eng. J.*, 2012, **211–212**, 302–309.